https://doi.org/10.20965/jrm.2015.p0032

Paper:

Landing Motion of a Legged Robot with Minimization of Impact Force and Joint Torque

Xianglong Wan, Takateru Urakubo, and Yukio Tada

Department of Systems Science, Graduate School of System Informatics, Kobe University
1-1 Rokkodai, Nada-ku, Kobe 657-8501, Japan
E-mail: man@opt.cs.kobe-u.ac.jp

[Received August 20, 2014; accepted November 17, 2014]

This paper deals with an optimal landing motion of a four-link legged robot that minimizes the impact force at the contact point and the joint torques necessary during the motion. The cost function for optimization is given as the weighted sum of the impact force and the joint torques. The configuration of the robot that is close to a singular configuration is advantageous in minimizing the joint torques for a heavy torso, while the configuration where the leg is bent is advantageous in reducing the impact force. This is shown by numerical optimization results with different weights for the cost function and a theoretical analysis of a simplified model of the robot.

Keywords: singular configuration, multi-objective optimization, motion planning, impact dynamics

1. Introduction

The development of the robots that can perform human-like movements has attracted many researchers [1–3]. Dynamic movements such as walking, running and jumping need coordination of many degrees of freedom under the gravitational force and the ground reaction force, and are difficult for robots to perform.

Especially, jumping is a highly dynamic motion and needs a large amount of energy in a short time because of large instantaneous ground reaction force and short duration. Several approaches to develop jumping robots have been proposed so far [4–8]. Most of them are based on the biological structure and biomechanics. In [4], biped robots with musculoskeletal system are constructed to realize a jumping motion from take-off to stable landing.

During a landing motion, large ground reaction force, called impact force, occurs due to the impact between the foot and the ground. Reducing the impact force (or momentum) is important for humans to prevent injuries and for robots to avoid mechanical breakdowns. When a robotic arm or leg collides with other object, the impact force caused by the collision depends on the configuration (posture) of the robot. The optimal configuration that minimizes the impact force can be calculated by using a mathematical model of the impact force. Two different impact force models have been considered in the references [9–11]. For the model in [9, 10], the impact with stiff objects occurs in an infinitesimally small period of time. The joint velocities and the momentum of the robot change discontinuously at the instant of collision. We call it *discontinuous model* in this paper. In [11], landing of a legged robot that has a foot equipped with a soft pad is considered. The soft pad generates a spring damper force between the foot and the ground. The impact through the pad occurs in a finite duration, and the changes in joint velocities and momentum of the robot are continuous. It is called *continuous model* in this paper. For both models, the configuration of the robot where the leg is bent, that is, the configuration far from the singular configuration where the leg is stretched out, is advantageous to reduce the impact force or momentum.

To complete a landing motion after the collision, joint torques of a legged robot have to bring the configuration to a stable stance and absorb the kinetic energy of the robot to stop the motion. The joint torques for human landing motion have been investigated so far. It was found in [12] that the joint stiffness alters during the ground-contact phase in human hopping. The leg stiffness modulation is sensitive to changes in ankle joint stiffness [13]. Inspired by those results, a body stiffness and damping control method has been proposed to achieve soft landing of a legged robot in [8]. Time varying stiffness and damping coefficients were optimized to reduce the peak value of ground reaction force.

On the other hand, minimization of necessary joint torques during a landing motion is also important for reducing the energy consumption of joint motors. More importantly, the weight of the robot can be reduced by using small motors if the necessary joint torques are small. The lighter weight makes the realization of a jumping robot much easier. In [14–16], we have shown that, for the task of pulling a heavy object with a two-link robot arm, joint torques can generate (or absorb) energy efficiently near singular configurations of the arm. Although the task does not include the collision with the object, this dynamic feature of singular configurations might be exploited for the landing motion of a legged robot; the initial configuration near singular configurations may be expected to be advantageous in absorbing the kinetic energy with small joint torques to stop the landing motion. In order to clar-

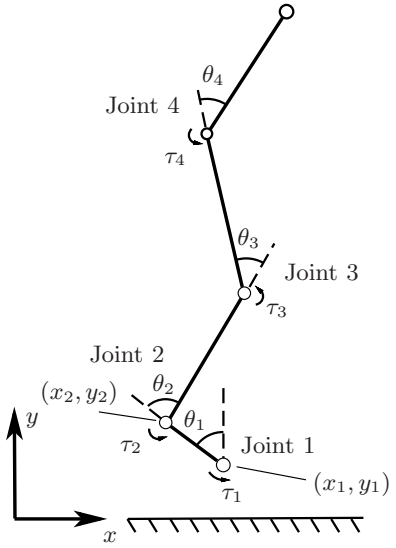

Fig. 1. Four-link legged robot.

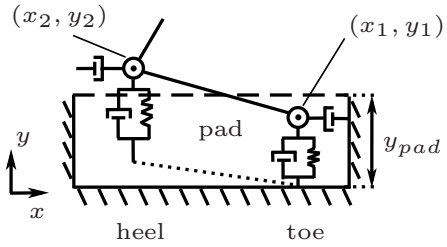

Fig. 2. Contact model.

ify the advantage, the dynamics around the impact near singular configurations has to be examined.

In this paper, we consider not only reduction of impact force but also minimization of joint torques for a landing motion of a four-link legged robot. To the best of our knowledge, the problem of optimizing them simultaneously during landing has not been dealt with in the literature. The landing motion that minimizes the peak value of the impact force and the necessary joint torques is obtained by numerical optimization. The cost function is composed of the weighted sum of the one for the impact force and the one for the joint torques. The impact force is calculated from the continuous model in a similar way as in [11] for the numerical optimization. Using the joint model proposed in [12], we assume that the joint torques are represented by the parameters in the stiffness and damping coefficients. Numerical optimization results show that, as the weight of the cost function for the joint torques increases, the optimal configuration of the robot at the impact time becomes close to the singular configuration. To verify and understand the results, a theoretical analysis of the dynamics around the impact is performed with a simple model of the legged robot where the discontinuous model of impact is used. The theoretical analysis provides new insight into landing motion; when the impact configuration is close to, but not exactly, the singular configuration, the joint velocity immediately after the impact has the maximum value, and the kinetic energy of the robot can be absorbed by small joint torques.

2. Four-Link Legged Robot

Let us consider the vertical landing of a one-legged planar robot (**Fig. 1**). The robot consists of four links, foot, lower limb, upper limb and torso, and they are called Link 1, Link 2, Link 3 and Link 4 respectively. We introduce a virtual joint which is located at the toe and call it *toe joint*. When the leg is in the landing phase, it is in contact with the ground through the toe or/and the heel. As shown in **Fig. 1**, the toe joint is called Joint 1, and the joint between Link i and $i+1$ is called Joint i ($i = 2,3,4$). A coordinate frame, (x,y), is chosen so that y-axis is along the vertical line and x-axis is on the horizontal ground. The positions of the toe and heel are denoted as $[x_1,y_1]^T$ and $[x_2,y_2]^T$. The angle and torque at Joint i are represented as θ_i and τ_i respectively, and they are positive in the counter-clockwise direction ($i = 1,2,3,4$). It is assumed that the toe joint freely rotates and the torque at the joint τ_1 is zero. The generalized coordinates and the generalized forces for the legged robot are expressed in vector forms as $\boldsymbol{q} = [x_1,y_1,\theta_1,\theta_2,\theta_3,\theta_4]^T$ and $\boldsymbol{\tau} = [0,0,0,\tau_2,\tau_3,\tau_4]^T$.

For a landing motion of the legged robot, we assume that, just before the contact with the ground, all the joint angular velocities are zero and the downward velocity of the robot is v_t. The initial values of generalized velocities are summarized as

$$\dot{\boldsymbol{q}}(0) = [0,-v_t,0,0,0,0]^T . \quad \ldots\ldots\ldots \quad (1)$$

2.1. Contact Model Between Foot and Ground

When the foot collides with the ground, an impact force acts at the contact point. For avoiding too large impacts and increasing the stability of movement, shock-absorbing mechanisms are often equipped under the feet of biped robots [11, 17, 18]. In this paper, we consider the foot equipped with a shock-absorbing pad. The interaction force between the foot and the ground is assumed to be obtained from a linear spring and damper model in the vertical direction and a linear damper model in the horizontal direction as shown in **Fig. 2**. It is also assumed that only the toe (Joint 1) and the heel (Joint 2) could be the contact points. The thickness of the pad is denoted as y_{pad}.

The interaction forces at the heel and the toe in the vertical direction are given by the following equation:

$$f_{yi} = \begin{cases} -k_y(y_i - y_{pad}) - d_y\dot{y}_i & \text{for } y_i < y_{pad} \\ 0 & \text{for } y_i \geq y_{pad} \end{cases} , \quad (2)$$

where k_y is a stiffness coefficient, d_y is a damping coefficient, and $i = 1$ and 2 for the toe and the heel respectively. Since the ground reaction force is never negative, the force f_{yi} is set to be zero if f_{yi} in Eq. (2) is negative.

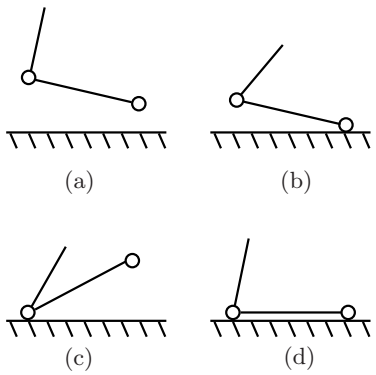

Fig. 3. Contact states: (a) no contact, (b) contact at toe, (c) contact at heel, (d) contact at toe and heel.

On the other hand, the interaction force in the horizontal direction can be expressed by

$$f_{xi} = \begin{cases} -d_x \dot{x}_i & \text{for } f_{yi} > 0 \\ 0 & \text{for } f_{yi} = 0 \end{cases} , \quad \ldots\ldots\ldots (3)$$

where d_x is a damping coefficient. Those interaction forces are written in a vector form as

$$\boldsymbol{F} = [f_{x1}, f_{y1}, f_{x2}, f_{y2}]^T . \quad \ldots\ldots\ldots (4)$$

2.2. Equations of Motion

The equations of motion for the legged robot can be described by

$$\boldsymbol{M}(\boldsymbol{q})\ddot{\boldsymbol{q}} + \boldsymbol{h}(\boldsymbol{q}, \dot{\boldsymbol{q}}) + \boldsymbol{\tau}_g = \boldsymbol{\tau} + \boldsymbol{J}^T \boldsymbol{F} , \quad \ldots\ldots (5)$$

where $\boldsymbol{M}(\boldsymbol{q})$ is the inertia matrix, $\boldsymbol{h}(\boldsymbol{q}, \dot{\boldsymbol{q}})$ is the vector with respect to the Coriolis and centrifugal effects, and $\boldsymbol{\tau}_g$ is the gravitational term. The matrix $\boldsymbol{J}$ is the Jacobian matrix with respect to the positions of the toe and the heel.

According to Eqs. (2) and (3), there exist four possible contact states between the foot and the ground as shown in **Fig. 3**. All the contact states are considered in the motion planning presented in the following section.

3. Optimal Landing Motion

3.1. Stiffness and Damping of Leg Joints

The joint torques for human motions are often expressed by joint stiffness and damping. In [12], the coefficients of stiffness and damping for human hopping have been examined in detail and a nonlinear stiffness model has been proposed. Based on the results in [12], we assume that the joint torques are represented as in the following form:

$$\tau_i = -K_i(\theta_i - \theta_{ie}) - D_i \dot{\theta}_i \ \ (\text{for } i = 2,3,4), \quad \ldots (6)$$

where the coefficients of stiffness and damping are given as

$$K_i = K_{i1} + K_{i2}(\theta_i - \theta_{is}) , \quad \ldots\ldots\ldots (7)$$

$$D_i = D_{i1} . \quad \ldots\ldots\ldots (8)$$

The angle θ_{is} is the angle of Joint i at the instant when the first contact between the foot and the ground occurs. The parameters K_{i1}, K_{i2}, D_{i1} and θ_{ie} determine the torque τ_i during the landing motion.

3.2. Optimization Problem

In this subsection, we formulate the optimization problem of finding the landing motion that reduces the peak vertical ground reaction force and minimizes the joint torques during the landing motion simultaneously. The following cost function is chosen as criterion for optimization:

$$J_C(\phi) = c_1 W_1 + W_2 , \quad \ldots\ldots\ldots (9)$$

where c_1 is the weight coefficient with respect to W_1. The functions W_1 and W_2 are defined as:

$$W_1 = \max_{t\in[0,T]}(f_{y1}(t) + f_{y2}(t)), \quad \ldots\ldots (10)$$

$$W_2 = \int_{t=0}^{T} \left((\tau_2)^2 + (\tau_3)^2 + (\tau_4)^2\right) dt , \quad \ldots\ldots (11)$$

where W_1 represents the peak value of vertical ground reaction force. The time t is set to be zero at the instant when the first contact between the foot and the ground occurs, and T denotes the end time of the landing motion.

In Eq. (9), ϕ represents the parameters for optimization and is chosen as the initial posture $\boldsymbol{\theta}(0) = (\theta_1(0), \theta_2(0), \theta_3(0), \theta_4(0))$, the coefficients K_{i1}, K_{i2}, D_{i1}, θ_{ie} $(i = 2,3,4)$ and the duration time T:

$$\phi = \{\boldsymbol{\theta}(0), K_{i1}, K_{i2}, D_{i1}, \theta_{ie}, T\} . \quad \ldots\ldots (12)$$

The initial posture is assumed to satisfy $0 \le \theta_1(0) < \pi/2$, that is, the first contact between the foot and the ground occurs in the state (b) shown in **Fig. 3**. After the first contact, the second and multiple contacts between the foot and the ground may happen in the state (b), (c) or (d).

At the end time of the motion, we put four constraints to the optimization problem. The horizontal position of the mass center of the robot should be above the foot at the end time $t = T$, which can be expressed as follows:

$$x_2 \le x_g(T) \le x_1 , \quad \ldots\ldots\ldots (13)$$

where x_g is the horizontal position of the mass center. The robot should be stationary at $t = T$:

$$\dot{\boldsymbol{q}}(T) = 0 . \quad \ldots\ldots\ldots (14)$$

The angle of the torso from the vertical direction should be small at $t = T$ so that the final posture of the robot is close to the one in human landing motion:

$$|\theta_t(T)| \le \frac{\pi}{4} , \quad \ldots\ldots\ldots (15)$$

where $\theta_t = \theta_1 + \theta_2 + \theta_3 + \theta_4$. The landing motion should be finished in 1 s:

$$T \le 1 . \quad \ldots\ldots\ldots (16)$$

3.3. Numerical Results

By changing the value of c_1, we can obtain the optimal solutions for the soft landing and the stiff one. The

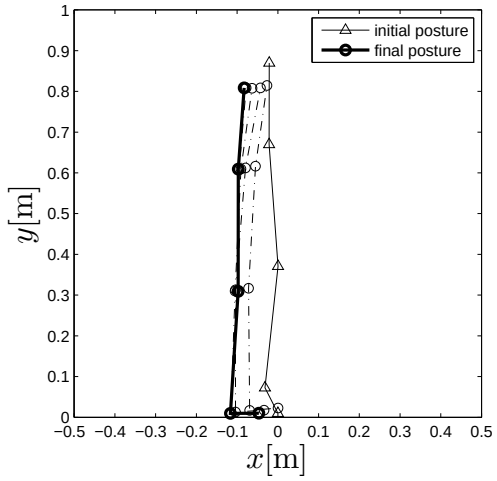

Fig. 4. Optimal motion of a legged robot (Case 1).

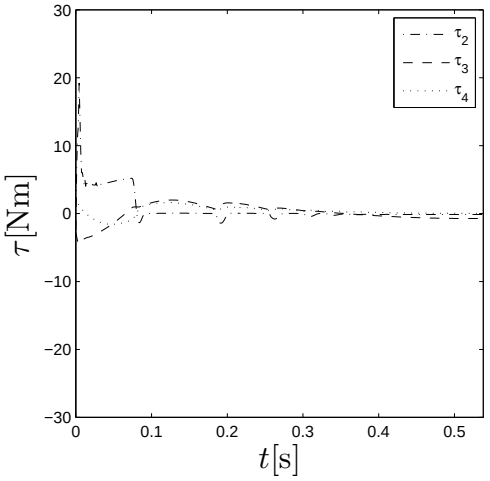

Fig. 6. Time histories of joint torques (Case 1).

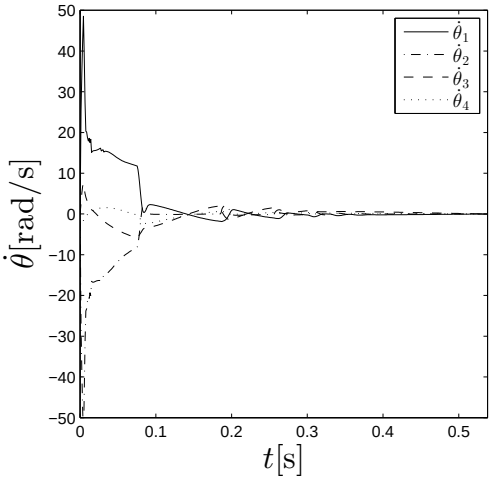

Fig. 5. Time histories of joint angular velocities (Case 1).

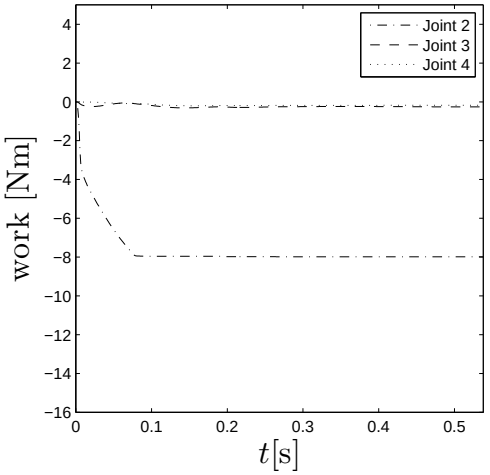

Fig. 7. Time histories of the work done by joint torques (Case 1).

solutions for different values of c_1 will be obtained by numerical optimization. To find the optimal values of J_C, the MATLAB function, fmincon, was used. The lengths of four links of the robot are chosen as 0.07 m, 0.3 m, 0.3 m and 0.2 m. The masses of the links are set to be 0.9 kg, 1.0 kg, 1.0 kg and 5 kg respectively. The thickness and parameters of the shock-absorbing pad are chosen as $y_{pad} = 0.01$ m, $k_y = 4.0 \times 10^5$ N/m, $d_y = 600$ Ns/m and $d_x = 500$ Ns/m respectively. The initial downward velocity of the robot v_t is set to be 1.5 m/s.

The numerical optimization was performed in two cases, Case 1 and Case 2, where the weight c_1 is set to be 0 and 1 respectively.

Case 1: $J_C = W_2$

The motion obtained by numerical simulation is shown in **Fig. 4** where the postures of the robot are drawn at every $T/5$ s. The time histories of joint angular velocities and joint torques are shown in **Figs. 5** and **6** respectively. The work done by each joint is calculated from them as shown in **Fig. 7**. The values of W_1 and W_2 for the obtained motion are 1192.3 N and 4.03 N^2m^2s. The optimal duration time T is 0.538 s.

From **Fig. 4**, the initial posture of the robot is close to the singular configuration that the leg is stretched out. After the first contact between the foot and the ground, the absolute values of $\dot{\theta}_2$ and τ_2 increase intensely in **Figs. 5** and **6**, while the others are relatively small during landing. Thus, the absolute value of work done by τ_2 is much larger than by τ_3 and τ_4 as in **Fig. 7**. That is, a large part of the kinetic energy of robot is absorbed at Joint 2 to stop the landing motion.

Case 2: $J_C = W_1 + W_2$

The motion obtained by numerical simulation is shown in **Fig. 8** where the postures of the robot are drawn at every $T/5$ s. **Figs. 9**, **10**, and **11** show the time histories of joint angular velocities, joint torques and work done by joint torques respectively. The values of W_1 and W_2 for the obtained motion are 377.4 N and 65.4 N^2m^2s. The optimal duration time T is 0.496 s.

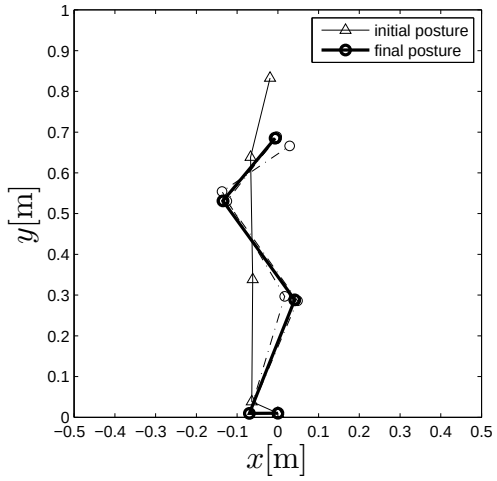

Fig. 8. Optimal motion of a legged robot (Case 2.)

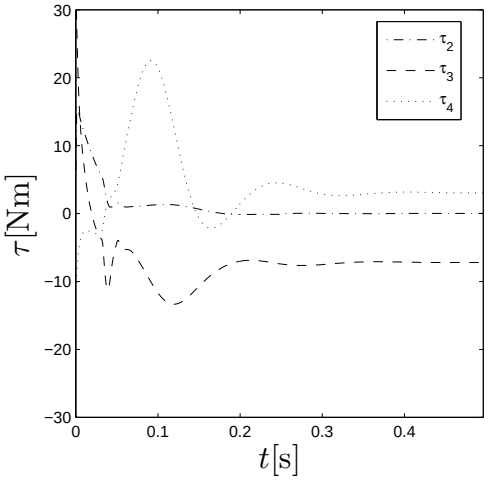

Fig. 10. Time histories of joint torques (Case 2).

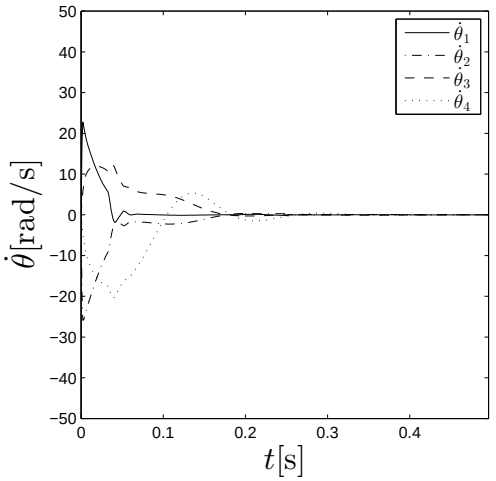

Fig. 9. Time histories of joint angular velocities (Case 2).

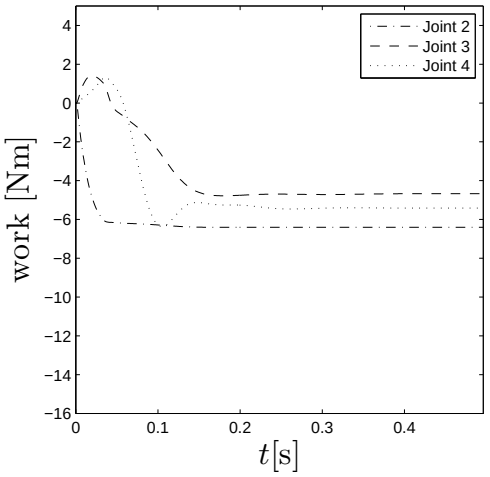

Fig. 11. Time histories of the work done by joint torques (Case 2).

At the initial posture, Joint 2 is flexed more than in Case 1. The impact force and the value of W_1 are smaller than in Case 1, while the joint torque τ_2 absorbs less energy. The energy of the robot is also absorbed by the joint torques τ_3 and τ_4 as shown in **Fig. 11**.

4. Impact Dynamics with a Simple Model

The numerical results in Section 3.3 show that the initial posture where Joint 2 is more flexed reduces the impact force, while the one with smaller θ_2 makes the time integral of joint torques smaller. The impact force has been investigated so far based on the discontinuous impact model where the impact occurs in an infinitesimally small period, and it is well known that flexed postures are advantageous in reducing the impact force [8]. In this section, we analyze the dynamic behavior of the robot at the impact instance by using a simplified model of the legged robot. The analytical results will explain not only the impact force but also the joint angular velocity right after the impact. For a larger joint angular velocity, the joint torque necessary to absorb the kinetic energy of the robot is smaller.

We consider a simple model of a legged robot as shown in **Fig. 12**. The leg is composed of two links, Links 1 and 2, and the torso is modeled as a heavy mass point attached at the top end of the leg. The mass and length of Link i are denoted as m_{ai} and l_{ai} respectively ($i = 1,2$), and the mass of the torso is m_w. The moment of inertia and the distance from Joint i to the center of mass for Link i are expressed by I_{ai} and l_{gi}. The bottom end of the leg is supposed to be a contact point, and its position is expressed as $\boldsymbol{p}_b = [x_b, y_b]^T$. The position of the top end is denoted as $\boldsymbol{p}_e = [x_e, y_e]^T$. In a similar manner as in Section 2, the angles and the joint torques are denoted as θ_{ai} and τ_{ai} ($i = 1,2$), and expressed in vector forms as $\boldsymbol{\theta}_a = [\theta_{a1}, \theta_{a2}]^T$, $\boldsymbol{\tau}_a = [0, \tau_{a2}]^T$, noting that $\tau_{a1} = 0$. The generalized coordinates and generalized forces for the system can be represented as $\boldsymbol{q} = [\boldsymbol{p}_b^T, \boldsymbol{\theta}_a^T]^T$ and $\boldsymbol{\tau} = [0,0,0,\tau_{a2}]^T$.

The variables just before and after the collision with

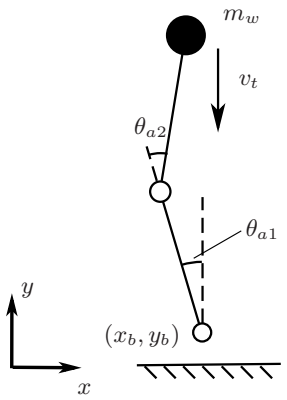

Fig. 12. Simple model of a legged robot with a heavy mass point (torso).

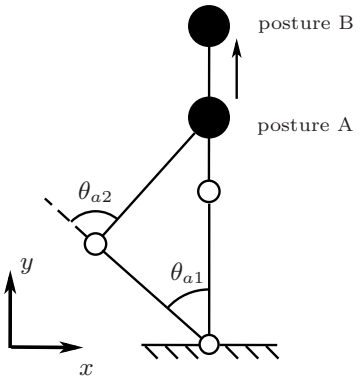

Fig. 13. Range of postures: from posture A to posture B.

the ground are denoted by superscripts $-$ and $+$ respectively. Similarly as in Eq. (1), the generalized velocities are chosen as $\dot{\boldsymbol{\theta}}_a^- = [0,0]^T$ and $\dot{\boldsymbol{p}}_b^- = [0,-v_t]^T$. The angular velocity $\dot{\boldsymbol{\theta}}_a^+$ and the impulse applied at the contact point will be analyzed under the following assumptions:

1) A perfectly inelastic collision occurs; the velocity of the bottom end of the robot becomes zero just after collision, that is, $\dot{\boldsymbol{p}}_b^+ = [0,0]^T$.
2) The mass of the torso is much larger than the ones of Links 1 and 2, namely, $m_w \gg m_{a1}, m_{a2}$.

The equation of motion for the robot is expressed as follows:

$$\boldsymbol{M}(\boldsymbol{q})\ddot{\boldsymbol{q}} + \boldsymbol{h}(\boldsymbol{q},\dot{\boldsymbol{q}}) + \boldsymbol{\tau}_g = \boldsymbol{\tau} + \boldsymbol{J}_b^T \boldsymbol{F} \ , \quad . \ . \ . \ . \quad (17)$$

where

$$\boldsymbol{M} = \begin{bmatrix} \boldsymbol{M}_1 & \boldsymbol{M}_2 \\ \boldsymbol{M}_2^T & \boldsymbol{M}_3 \end{bmatrix} , \quad . \ . \ . \ . \ . \ . \ . \ . \ . \quad (18)$$

$$\boldsymbol{M}_1 = \begin{bmatrix} m_{a1}+m_{a2}+m_w & 0 \\ 0 & m_{a1}+m_{a2}+m_w \end{bmatrix}, \quad (19)$$

$$\boldsymbol{M}_2 = m_{a1}\boldsymbol{J}_{g1} + m_{a2}\boldsymbol{J}_{g2} + m_w \boldsymbol{J}_e, \quad . \ . \ . \ . \ . \quad (20)$$

$$\boldsymbol{M}_3 = \boldsymbol{M}_a + m_w \boldsymbol{J}_e^T \boldsymbol{J}_e. \quad . \ . \ . \ . \ . \ . \ . \ . \quad (21)$$

The matrix $\boldsymbol{M}_a$ is the inertia matrix of the leg composed of two links, and does not include the inertia of the heavy mass point. The matrices $\boldsymbol{J}_b, \boldsymbol{J}_{g1}, \boldsymbol{J}_{g2}, \boldsymbol{J}_e$ are the Jacobian matrices with respect to $\boldsymbol{p}_b$, the mass centers of Link 1 and Link 2, and $\boldsymbol{p}_e$, respectively. Note that $\boldsymbol{J}_b$ and $\boldsymbol{J}_e$ are expressed as

$$\boldsymbol{J}_b = \begin{bmatrix} 1 & 0 & 0 & 0 \\ 0 & 1 & 0 & 0 \end{bmatrix} , \quad . \ . \ . \ . \ . \ . \ . \ . \ . \quad (22)$$

$$\boldsymbol{J}_e = -\begin{bmatrix} \mathrm{c}\theta_{a1} & -\mathrm{s}\theta_{a1} \\ \mathrm{s}\theta_{a1} & \mathrm{c}\theta_{a1} \end{bmatrix} \begin{bmatrix} l_{a1}+l_{a2}\mathrm{c}\theta_{a2} & l_{a2}\mathrm{c}\theta_{a2} \\ l_{a2}\mathrm{s}\theta_{a2} & l_{a2}\mathrm{s}\theta_{a2} \end{bmatrix} , \quad (23)$$

where $\mathrm{c}*$ and $\mathrm{s}*$ mean $\cos(*)$ and $\sin(*)$. The vector $\boldsymbol{F} = [F_y, F_y]^T$ is the ground reaction force.

In a similar way as in [9], we assume that the impact with the ground occurs in an infinitesimally small period of time δt and a finite translational momentum $\bar{\boldsymbol{F}}$ is supplied from $\boldsymbol{F}$ during the period. Integrating Eq. (17) during the period, we obtain the following equation:

$$\lim_{\delta t \to 0} \int_{t=0}^{\delta t} (\boldsymbol{M}(\boldsymbol{q})\ddot{\boldsymbol{q}} + \boldsymbol{h}(\boldsymbol{q},\dot{\boldsymbol{q}}) + \boldsymbol{\tau}_g) = \lim_{\delta t \to 0} \int_{t=0}^{\delta t} (\boldsymbol{\tau} + \boldsymbol{J}_b^T \boldsymbol{F}). \quad . \ . \ . \ . \ . \ . \ . \quad (24)$$

The above equation is rewritten as

$$\boldsymbol{M}(\boldsymbol{q})(\dot{\boldsymbol{q}}^+ - \dot{\boldsymbol{q}}^-) = \boldsymbol{J}_b^T \bar{\boldsymbol{F}}. \quad . \ . \ . \ . \ . \ . \ . \quad (25)$$

From the assumption 1) and Eq. (25), the impulse $\bar{\boldsymbol{F}}$ is derived as

$$\bar{\boldsymbol{F}} = -(\boldsymbol{J}_b \boldsymbol{M}^{-1} \boldsymbol{J}_b^T)^{-1} \boldsymbol{J}_b \dot{\boldsymbol{q}}^- . \quad . \ . \ . \ . \ . \ . \ . \quad (26)$$

By substituting Eq. (26) into Eq. (25), $\dot{\boldsymbol{q}}^+$ is obtained as

$$\dot{\boldsymbol{q}}^+ = (I_{4\times 4} - \boldsymbol{M}^{-1}\boldsymbol{J}_b^T (\boldsymbol{J}_b \boldsymbol{M}^{-1} \boldsymbol{J}_b^T)^{-1} \boldsymbol{J}_b) \dot{\boldsymbol{q}}^- . \quad (27)$$

By using Eqs. (18) and (22), the impulse and the joint angular velocity just after the collision are represented as

$$\begin{aligned} \bar{\boldsymbol{F}} &= -(\boldsymbol{M}_1 - \boldsymbol{M}_2 \boldsymbol{M}_3^{-1} \boldsymbol{M}_2^T) \dot{\boldsymbol{p}}_b^- \\ &= -(\boldsymbol{M}_1 \dot{\boldsymbol{p}}_b^- - \boldsymbol{M}_2 \dot{\boldsymbol{\theta}}_a^+) , \quad . \ . \ . \ . \ . \ . \ . \quad (28) \end{aligned}$$

$$\dot{\boldsymbol{\theta}}_a^+ = \boldsymbol{M}_3^{-1} \boldsymbol{M}_2^T \dot{\boldsymbol{p}}_b^- . \quad . \ . \ . \ . \ . \ . \ . \ . \ . \quad (29)$$

From Eqs. (28) and (29), the values of $\bar{\boldsymbol{F}}$ and $\dot{\boldsymbol{\theta}}_a^+$ are varied by the posture of the robot $\boldsymbol{\theta}_a$ and the link parameters such as l_{a1} and l_{a2}. The solutions of $\bar{\boldsymbol{F}}$ and $\dot{\boldsymbol{\theta}}_a^+$ in Eqs. (28) and (29) are a little complicated to understand their variations for all the joint angles $\boldsymbol{\theta}_a$ and all the link lengths l_{a1} and l_{a2}. In this section, we will investigate their variations under the following conditions:

$$l_{a1} = l_{a2}, \ \theta_{a2} = -2\theta_{a1}, \ 0 \le \theta_{a1} \le \frac{\pi}{4} \text{ rad} . \ . \ . \quad (30)$$

The posture of the robot with the conditions can be changed from posture A to posture B as shown in **Fig. 13**, keeping the position of the mass point just above the contact point. For posture B, the leg is in the singular configuration with $\theta_{a1} = 0$ rad and the matrix $\boldsymbol{J}_e$ is singular.

From the assumption 2), Eqs. (29) and (30), the approx-

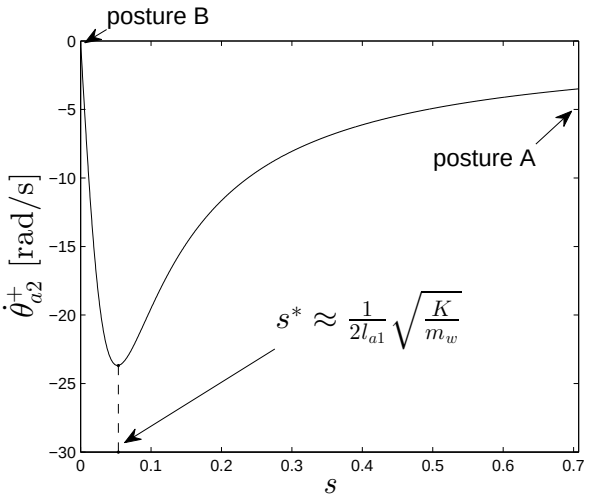

Fig. 14. Variation of $\dot{\theta}^+_{a2}$ with respect to s.

imate solution of $\dot{\boldsymbol{\theta}}^+_a$ can be obtained as

$$\dot{\boldsymbol{\theta}}^+_a = \begin{bmatrix} \dot{\theta}^+_{a1} \\ \dot{\theta}^+_{a2} \end{bmatrix} \approx \begin{bmatrix} \dfrac{2m_w l_{a1} v_t s(1-s^2)}{4m_w l^2_{a1} s^2(1-s^2)+K} \\ \dfrac{-4m_w l_{a1} v_t s(1-s^2)}{4m_w l^2_{a1} s^2(1-s^2)+K} \end{bmatrix}, \quad (31)$$

where $K = m_{a1} l^2_{g1} + m_{a2}(l_{a1} - l_{g2})^2 + I_{a1} + I_{a2}$ and the variable s is defined as $s = \sin\theta_{a1}$. Under Eq. (30), the range of s satisfies $0 \le s \le \sqrt{2}/2$. Posture A and posture B correspond to $s = \sqrt{2}/2$ and $s = 0$ respectively. By substituting Eq. (31) into Eq. (28), the vertical impulse $\bar{F}_y$ can be approximately calculated as

$$\bar{F}_y \approx m_w v_t - \frac{4m^2_w l^2_{a1} v_t s^2(1-s^2)}{4m_w l^2_{a1} s^2(1-s^2)+K}. \quad \ldots (32)$$

Furthermore, the kinetic energy of the robot just after the collision, $E^+ = (\dot{\boldsymbol{\theta}}^{+T}_a \boldsymbol{M}_3 \dot{\boldsymbol{\theta}}^+_a)/2$, can be calculated from Eq. (31) as

$$E^+ \approx \frac{2m^2_w l^2_{a1} v^2_t s^2(1-s^2)}{4m_w l^2_{a1} s^2(1-s^2)+K} \approx \frac{1}{2} v_t (m_w v_t - \bar{F}_y). \quad (33)$$

From Eq. (31), the variation of $\dot{\boldsymbol{\theta}}^+_a$ can be seen explicitly. Noting that $\dot{\theta}^+_{a2} = -2\dot{\theta}^+_{a1}$ in Eq. (31), we focus on the behavior of $\dot{\theta}^+_{a2}$ below. The absolute value of $\dot{\theta}^+_{a2}$ is zero at $s = 0$, and sharply increases as s becomes slightly larger. The peak of $|\dot{\theta}^+_{a2}|$ occurs at $s = s^*$ where

$$s^* \approx \frac{1}{2l_{a1}}\sqrt{\frac{K}{m_w}}. \quad \ldots (34)$$

As s approaches $\sqrt{2}/2$ from s^*, $|\dot{\theta}^+_{a2}|$ monotonically decreases. Therefore, $|\dot{\theta}^+_{a2}|$ has the maximum value for the posture where $s = s^*$. Since s^* is small from Eq. (34) and the assumption 2), the posture is close to posture B where the leg is in a singular configuration. As a result, $|\dot{\theta}^+_{a2}|$ has the maximum value at the posture close to the singular posture B, while it is zero at posture B. The profile of $\dot{\theta}^+_{a2}$ as a function of s is drawn in **Fig. 14**, by using the physical parameters in **Table 1**.

Table 1. Physical parameters for the simple model.

l_{a1}	0.6 m	l_{a2}	0.6 m
l_{g1}	0.3 m	l_{g2}	0.3 m
I_{a1}	0.01 kgm^2	I_{a2}	0.01 kgm^2
m_{a1}	1 kg	m_{a2}	1 kg
m_w	50 kg	v_t	1.5 m/s

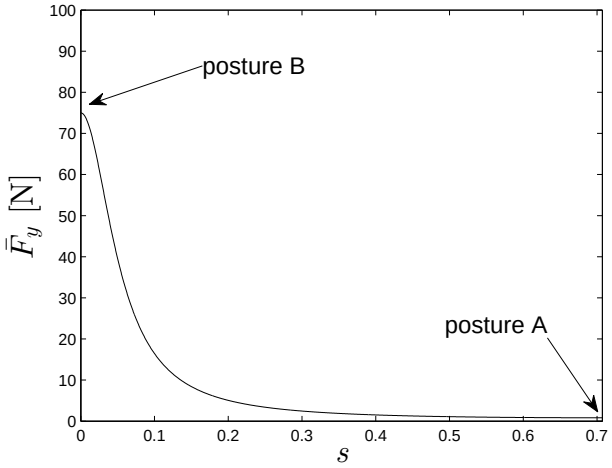

Fig. 15. Variation of $\bar{F}_y$ with respect to s.

From Eq. (32), $\bar{F}_y$ has the maximum value at $s = 0$, and monotonically decreases as s approaches $\sqrt{2}/2$. That is to say, $\bar{F}_y$ increases as the posture becomes close to the singular posture B. **Fig. 15** shows the profile $\bar{F}_y$ as a function of s by using the physical parameters in **Table 1**.

Moreover, the similar behavior of $\dot{\theta}^+_{a2}$ and $\bar{F}_y$ can be obtained, even if $\theta_{a2} \neq -2\theta_{a1}$ and $l_{a1} \neq l_{a2}$. This is easily verified by calculating their variations numerically by using Eqs. (28) and (29).

As the above results, the posture where the leg is bent is advantageous in reducing the impulse $\bar{F}_y$ that would correspond to W_1 in Section 3. On the other hand, the posture around $s = s^*$ can be useful for reducing the joint torques necessary for the landing motion. For the simple model, the rate of work done by joint torques after the impact can be expressed as

$$P_a = \boldsymbol{\tau}^T_a \dot{\boldsymbol{\theta}}_a = \tau_{a2} \dot{\theta}_{a2}. \quad \ldots (35)$$

Since $|\dot{\theta}^+_{a2}|$ has the maximum value at $s = s^*$, the kinetic energy of the robot can be absorbed most efficiently by τ_{a2}. The kinetic energy E^+ also depends on the posture as in Eq. (33). For the posture with $s = s^*$, a part of the kinetic energy $E^- = (m_{a1} + m_{a2} + m_w) v^2_t/2$ is eliminated by the inelastic collision with the ground, while almost all the energy E^- remains as E^+ for the posture close to posture A. Therefore, the posture around $s = s^*$, that is close to the singular posture B, is advantageous in reducing the joint torque τ_{a2} that would correspond to W_2 in Section 3.

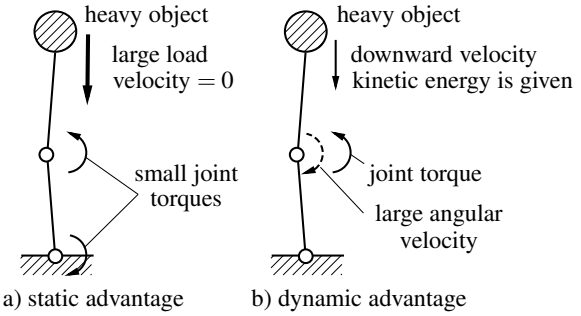

Fig. 16. Advantages of singular configuration for a two-link robot.

5. Discussion

From the numerical results in Case 1 and the theoretical results in Section 4, the amount of joint torques necessary for the landing motion is reduced for the posture close to a singular one. Singular configurations of a two-link robot have two kinds of advantages in achieving tasks such as holding and pulling heavy objects as shown in **Fig. 16**. One is the advantage in statics; the robot can sustain a large load at the end effector with small joint torques near the singular configuration [19, 20]. The other is the advantage in dynamics; the joint torques can absorb (or generate) energy the most efficiently, if the robot is in the singular configuration and the motion of the heavy object is vertical [14–16].

As mentioned in Section 4, the kinetic energy E^+ for the simple model depends on the posture as in Eq. (33). For posture B where $s = 0$, E^+ becomes zero, though the impulse $\bar{F}_y$ has the maximum value. From the assumption 1) of the perfectly inelastic collision, all the energy E^- is eliminated despite $\tau_{a2} = 0$. The corresponding motion for the four-link legged robot in Section 2 is the motion where all the joints of the robot are fully extended and the robot bounces on the ground multiple times until all the energy E^- is eliminated. Although $W_2 = 0$ for the motion, it was not found in the numerical optimization for Case 1 from the constraints (14) and (16). Instead, for the motion obtained in Case 1, non-zero E^+ is provided to the robot at the posture around $s = s^*$, and W_2 is reduced by using the dynamic advantage.

Regarding the subsystem composed of three links, Links 2, 3 and 4, as one link, the four-link legged robot can be considered as a simple model composed of Link 1 and the subsystem. From Eq. (29), we can obtain numerically the value of θ_{a1} that maximizes $|\dot{\theta}_{a2}^+|$ for the simple model. The obtained value θ_{a1}^* is 0.69 rad, while the corresponding values in Cases 1 and 2 are 0.47 rad and 1.15 rad. In Case 1, θ_1 at the initial posture is close to θ_{a1}^*, $|\dot{\theta}_2^+|$ $\left(\approx |\dot{\theta}_{a2}^+|\right)$ becomes large after collision as shown in **Fig. 5**, and the joint torque τ_2 absorbs the kinetic energy of the robot efficiently as shown in **Fig. 7**. On the other hand, in Case 2, $|\dot{\theta}_2^+|$ is much smaller than in Case 1 as shown in **Fig. 9**. The absorption of energy at Joint 2 is not sufficient to stop the motion of the robot, and the torques τ_3 and τ_4 also absorb the energy as shown in **Fig. 11**.

It should be noted that the value of cost function W_2 also depends on the posture of the robot around the end time. Since the robot is in the contact state (d) around the end time, the posture of the subsystem composed of Links 2, 3 and 4 affects highly the joint torques necessary to sustain the heavy torso. In Case 1, the posture of the subsystem is kept near the singular posture where the three links are aligned in a straight line, and the joint torques become very small around the end time from the static advantage of singular configurations as shown in **Fig. 6**. In Case 2, the posture of the subsystem is far from the singular one around the end time, and large joint torques continue to be required as shown in **Fig. 10**.

Moreover, optimization results for other values of c_1 show that, as the value of c_1 approaches 0, the obtained optimal motion becomes similar to the one in Case 1. For the value of c_1 larger than 1, the optimal motion is almost the same as in Case 2.

6. Conclusion

In this paper, we solved the optimal landing problem for a four-link legged robot where the cost function is chosen as a weighted sum of the peak vertical ground reaction force and the joint torques during the motion. Numerical optimization results with different weights for the cost function show that the posture of the leg close to a singular posture is useful for reducing the joint torques during landing, while the flexion of the leg is advantageous for reducing the reaction force. Those results were explained by a theoretical analysis for a simplified model of the legged robot.

References:

[1] K. Hirai, M. Hirose, Y. Haikawa, and T. Takenaka, "The development of Honda humanoid robot," Proc. of 1998 IEEE Int. Conf. on Robotics and Automation, Vol.2, pp. 1321-1326, 1998.

[2] T. Kanda, H. Ishiguro, M. Imai, and T. Ono, "Body Movement Analysis of Human-Robot Interaction," Int. Joint Conf. on Artificial Intelligence, pp. 177-182, 2003.

[3] J. Urata, Y. Nakanishi, K. Okada, and M. Inaba, "Design of high torque and high speed leg module for high power humanoid," Proc. of IEEE/RSJ Int. Conf. on Intelligent Robots and Systems, pp. 4497-4502, 2010.

[4] R. Niiyama, A. Nagakubo, and Y. Kuniyoshi, "Mowgli: A Bipedal Jumping and Landing Robot with an Artificial Musculoskeletal System," Proc. of IEEE Int. Conf. on Robotics and Automation, pp. 2546-2551, 2007.

[5] R. Niiyama, S. Nishikawa, and Y. Kuniyoshi, "Biomechanical Approach to Open-Loop Bipedal Running with a Musculoskeletal Athlete Robot," Advanced Robotics, Vol.26, No.3-4, pp. 383-398, 2012.

[6] K. Arikawa and T. Mita, "Design of multi-DOF jumping robot," Proc. of IEEE Int. Conf. on Robotics and Automation, Vol.4, pp. 3992-3997, 2002.

[7] S. Hyon and T. Mita, "Development of a biologically inspired hopping robot – Kenken," Proc. of IEEE Int. Conf. on Robotics and Automation, pp. 3984-3991, 2002.

[8] S. Sung and Y. Youm, "Landing Motion Control of Articulated Legged Robot," Proc. of IEEE Int. Conf. on Robotics and Automation, pp. 3230-3236, 2007.

[9] I. D. Walker, "The use of kinematic redundancy in reducing impact and contact effects in manipulation," Proc. of IEEE Int. Conf. on Robotics and Automation, Vol.1, pp. 434-439, 1990.

[10] I. D. Walker, "Impact configurations and measures for kinematically redundant and multiple robot systems," IEEE Trans. on Robotics and Automation, Vol.10, pp. 670-683, 1994.

[11] J. H. Park and H. Chung, "Impedance Control and Modulation for Stable Footing in Locomotion of Biped Robots," Proc. of IEEE/RSJ Int. Conf. on Intelligent Robots and Systems, Vol.3, pp. 1786-1791, 1999.
[12] J. Mizrahi, E. Kimmel, O. Verbitsky, and E. Isakov, "Constant and Variable Stiffness and Damping of the Leg Joints in Human Hopping," J. of Biomechanical Engineering, Vol.125, pp. 507-514, 2003.
[13] C. T. Farley and D. C. Morgenroth, "Leg stiffness primarily depends on ankle stiffness during human hopping," J. of Biomechanical Engineering, Vol.32, pp. 267-273, 1999.
[14] T. Urakubo, T. Mashimo, and T. Kanade, "Efficient pulling motion of a two-link robot arm near singular configuration," Proc. of IEEE/RSJ Int. Conf. on Intelligent Robots and Systems, pp. 1372-1377, 2010.
[15] T. Urakubo, T. Mashimo, and T. Kanade, "Optimal placement of a two-link manipulator for door opening," Proc. of IEEE/RSJ Int. Conf. on Intelligent Robots and Systems, pp. 1446-1451, 2009.
[16] T. Urakubo, H. Yoshioka, T. Mashimo, and X. Wan, "Experimental Study on Efficient Use of Singular Configuration in Pulling Heavy Objects with Two-link Robot Arm," Proc. of IEEE Int. Conf. on Robotics and Automation, pp. 4582-4587, 2014.
[17] S. Nakaoka, S. Hattori, F. Kanehiro, S. Kajita, and H. Hirukawa, "Constraint-based dynamics simulator for humanoid robots with shock absorbing mechanisms," Proc. of IEEE/RSJ Int. Conf. on Intelligent Robots and Systems, pp. 3641-3647, 2007.
[18] J. Yamaguchi, A. Takanishi, and I. Kato, "Experimental development of a foot mechanism with shock absorbing material for acquisition of landing surface position information and stabilization of dynamic biped walking," Proc. of IEEE Int. Conf. on Robotics and Automation, Vol.3, pp. 2892-2899, 1995.
[19] V. Kumar and J. F. Gardner, "Kinematics of Redundantly Actuated Closed Chains," IEEE Trans. on Robotics and Automation, Vol.6, No.2, pp. 269-274, 1990.
[20] K. L. Brown, "Design and Analysis of Robots that Perform Dynamic Tasks Using Internal Body Motion," Ph.D. Thesis, MIT, 1994.

Name:
Xianglong Wan

Affiliation:
Ph.D. Student, Department of Systems Science, Graduate School of System Informatics, Kobe University

Address:
1-1 Rokkodai, Nada-ku, Kobe 657-8501, Japan

Brief Biographical History:
2009 Received B.S. degree in Engineering from Huazhong University of Science and Technology, China
2012 Received M.S. degree in System Informatics from Kobe University

Membership in Academic Societies:
- The Institute of Electrical and Electronics Engineers (IEEE) Robotics and Automation Society (RAS)
- The Robotics Society of Japan (RSJ)

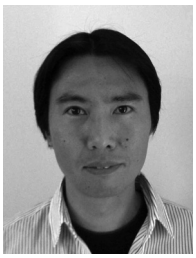

Name:
Takateru Urakubo

Affiliation:
Assistant Professor, Department of Systems Science, Graduate School of System Informatics, Kobe University

Address:
1-1 Rokkodai, Nada-ku, Kobe 657-8501, Japan

Brief Biographical History:
2001- Research Associate, Faculty of Engineering, Kobe University
2007-2009 Visiting Scientist, Carnegie Mellon University
2010- Assistant Professor, Graduate School of System Informatics, Kobe University

Main Works:
- "Attitude Control of a Spacecraft with Two Reaction Wheels," J. of Vibration and Control, Vol.10, Issue 9, pp. 1291-1311, 2004.

Membership in Academic Societies:
- The Institute of Electrical and Electronics Engineers (IEEE)
- The Society of Instrument and Control Engineers (SICE)
- The Robotics Society of Japan (RSJ)
- The Institute of Systems, Control and Information Engineers (ISCIE)

Name:
Yukio Tada

Affiliation:
Professor, Department of Systems Science, Graduate School of System Informatics, Kobe University

Address:
1-1 Rokkodai, Nada-ku, Kobe 657-8501, Japan

Brief Biographical History:
1995- Professor, Faculty of Engineering, Kobe University
2010- Professor, Graduate School of System Informatics, Kobe University

Main Works:
- Y. Tada and Y. Seguchi, "Shape Determination of Structures Based on the Inverse Variational Principle / The Finite Element Approach," Ch.8 of New Directions in Optimum Structural Design, pp. 197-209, John Wiley, 1984.
- Y. Tada and T. Nagashima, "Modeling and Simulation of Brain Lesions by the Finite-Element Method," IEEE Engineering in Medicine and Biology, Vol.13, No.4, pp. 497-503, 1994.
- M. Muromaki and Y. Tada, "Shape Design of Flexible Arm Considering Control Performance," Proc. of 9th World Congress on Structural and Multidisciplinary Optimization, paper144_1, pp. 1-6, 2011.

Membership in Academic Societies:
- International Society for Structural and Multidisciplinary Optimization (ISSMO)
- The Japan Society of Mechanical Engineers (JSME)
- The Institute of Systems, Control and Information Engineers (ISCIE)